



รายงานวิจัยฉบับสมบูรณ์

โครงการแนวทางใหม่ของการประสานภาพที่ความเร็วสูง ของกล้องจุลทรรศน์เชิงแสงชนิดเกเบอร์

An alternative fusing algorithm for high speed Gabor domain optical coherence microscopy

โดย ดร.พนมศักดิ์ มีมนต์

พฤศจิกายน 2558

สัญญาเลขที่ TRG5680091

รายงานวิจัยฉบับสมบูรณ์

โครงการแนวทางใหม่ของการประสานภาพที่ความเร็วสูง ของกล้องจุลทรรศน์เชิงแสงชนิดเกเบอร์

An alternative fusing algorithm for high speed Gabor domain optical coherence microscopy

ผู้วิจัย ดร.พนมศักดิ์ มีมนต์ มหาวิทยาลัยเทคโนโลยีสุรนารี

สนับสนุนโดยสำนักงานกองทุนสนับสนุนการวิจัยและต้นสังกัด

(ความเห็นในรายงานนี้เป็นของผู้วิจัย สกว.และต้นสังกัดไม่จำเป็นต้องเห็นด้วยเสมอไป)

ABSTRACT

Project Code: TRG5680091

Project Title: An alternative fusing algorithm for high speed Gabor domain optical coherence

microscopy

Investigator: Dr. Panomsak Meemon

E-mail Address : panomsak@sut.ac.th

Project Period: 2.5 years (June 3, 2013 – November 31 2015)

To date, optical imaging technology plays an important role in medical diagnostics and treatments. It also has applications in guiding the biopsy and surgery. The main advantages of optical imaging are its high-resolution high-speed and noninvasive capability. Optical coherence tomography (OCT) is one of emerging optical imaging technologies that is capable of in vivo microscopic cross-sectional imaging of biological tissues and organs. Particularly, one outstanding capability of OCT is the ability to provide depth-section of the sample at high resolution and sensitivity. Recently, the development of Gabor-domain optical coherence microscopy (GD-OCM), one of many variations of OCT techniques, was introduced. GD-OCM combines the high speed imaging capability of the frequency domain OCT (FD-OCT) and the ability to dynamically refocus of the liquid-lens based dynamic focus microscope developed by the team of scientists at the University of Rochester. GD-OCM acquires multiple cross-sectional images at different focus position of the objective lens and then fuses them together to obtain invariant high resolution 3D image of the sample. However, this 3D high resolution dataset comes with the cost of processing time that involves a massive amount of Fourier transformations. This project aims to address this issue by developing an alternative Gabor-based fusing algorithm that will dramatically improve the processing speed of the GD-OCM and hence enable 3D high resolution imaging of biological samples in real time. The developed algorithm will help moving the technology of GD-OCM one step closer to clinical diagnostic tools in the future.

Keywords : optical coherence tomography, optical coherence microscopy, microscopic imaging, 3D imaging, Gabor transform, Gabor filtering, spectral interference

าเทคัดย่อ

รหัสโครงการ: TRG5680091

ชื่อโครงการ: แนวทางใหม่ของการประสานภาพที่ความเร็วสูงของกล้องจุลทรรศน์เชิงแสงชนิดเกเบอร์

ชื่อหักวิจัย: ดร. พนมศักดิ[์] มีมนต์

E-mail Address: panomsak@sut.ac.th

ระยะเวลาโครงการ: 2 ปี 6 เดือน (ตั้งแต่ 3 มิถุนายน 2556 ถึง 31 พฤศจิกายน 2558)

ปัจจุบัน เทคโนโลยีการถ่ายภาพเชิงแสงมีบทบาทอย่างมากสำหรับช่วยในการวินิจฉัยและการ รักษาทางการแพทย์ อีกทั้ง ยังมีบทบาทสำคัญในการถ่ายภาพเพื่อใช้เป็นข้อมูลในการผ่าตัด จุดเด่น สำคัญของการถ่ายภาพเชิงแสงคือความละเอียดในระดับไมครอนและความเร็วของการถ่ายภาพที่สูง อีก ทั้ง ไม่ก่อให้เกิดอันตรายใดๆ ต่อเซลล์สิ่งมีชีวิต ระบบถ่ายภาพตัดขวางเชิงแสงแบบออพติกคัลโคเฮีย เรนซ์โทโมกราฟฟี หรือ OCT เป็นอีกหนึ่งเทคโนโลยีใหม่ของการถ่ายภาพเชิงแสงเพื่อใช้ประโยชน์ ซึ่งมีลักษณะภาพถ่ายที่ได้คล้ายภาพอัลตร้าชาวด์แต่ทว่าให้ความละเอียดในระดับ กล้องจุลทรรศน์ ในปัจจุบัน ได้มีการพัฒนาระบบโอซีทีขึ้นหลากหลายรูปแบบ ซึ่งมีฟังก์ชันการทำงาน และความสามารถในการถ่ายภาพที่แตกต่างกันออกไป และในช่วงเกือบ 10 ปีที่ผ่านมา ได้มีแนวคิดใหม่ ของการถ่ายภาพแบบโอซีที่ซึ่งใช้ชื่อว่า เกเบอร์โดเมนออพติกคัลโคเฮียเรนซ์ไมโครสโคป หรือเรียกย่อๆ ว่า GD-OCM ซึ่งเป็นระบบที่รวมความสามารถด้านความเร็วในการถ่ายภาพของระบบโอซีที่ในโดเมน ความถี่และความสามารถในการปรับระยะโฟกัสของโพรบถ่ายภาพที่ออกแบบมาโดยเฉพาะโดยทีมวิจัย ของมหาวิทยาลัยโรสเชสเตอร์ GD-OCM ถ่ายภาพหลายๆ ภาพที่ตำแหน่งเดียวกัน แต่ว่าปรับตำแหน่ง โฟกัสของเลนส์ถ่ายภาพให้ต่างกันในแต่ละภาพที่ถ่ายตามความลึก จากนั้นนำภาพที่ถ่ายได้ทั้งหมดมา ประมวลผลร่วมกันเพื่อตัดเอาเฉพาะส่วนที่มีความคมชัดของแต่ละภาพออกมา แล้วรวมเข้าด้วยกันเป็น หนึ่งภาพที่มีความคมชัดตลอดทั้งภาพ อย่างไรก็ตาม ความสามารถดังกล่าวมาพร้อมกับระยะเลาในการ ประมวลสัญญาณที่เพิ่มขึ้นหลายเท่าตัวเมื่อเทียบกับระบบ OCT แบบปกติ ดังนั้น ในโครงการนี้ ทีมผู้วิจัย ได้พัฒนาแนวทางใหม่ของการประสานภาพในระบบ GD-OCM โดยใช้หลักการของการประสานภาพใน โดเมนความถี่ ซึ่งจะสามารถประมวลผลภาพได้เร็วขึ้นจากเดิมกว่าเท่าตัว ทั้งนี้ ความสามารถในการ ประมวลผลได้เร็วขึ้นนี้ คาดว่าจะสามารถพัฒนาต่อยอดเพื่อให้ระบบ GD-OCM สามารถถ่ายภาพได้แบบ เวลาจริงต่อไป ซึ่งจะทำให้สามารถประยุกต์ใช้งานได้กว้างขวางขึ้น

Keywords: ออพติกคัลโคเฮียเรนซ์โทโมกราฟฟี, ออพติกคัลโคเฮียเรนซ์ไมโครสกอปี, กล้องจุลทรรศน์ สามมิติ, การแปลงสัญญาณแบบเกเบอร์, การประสานภาพแบบเกเบอร์, การแทรกสอดในโดเมนความถึ่

ACKNOWLEDGMENTS

I would like to gratefully acknowledge the Thailand Research Fund (TRF) and Suranaree University of Technology for funding this research. I would like to thank Prof. Dr. Joewono Widjaja at Suranaree University of Technology for his mentoring on this project. This work could not be completed without inputs from Prof. Dr. Jannick Rolland at the Institute of Optics, University of Rochester for stimulating discussion about the Gabor-based fusing technique.

TABLE OF CONTENTS

LIST O	F FIGURES	V
LIST O	F TABLES	vi
LIST O	F ACRONYMS/ABBREVIATIONS	vii
СНАРТ	ER One: INTRODUCTION	1
1.1	Introduction to the research problem and its significance	1
1.2	Literature review	2
1.3	Research Objectives	10
1.4	Methodology	10
СНАРТ	ER Two: SPECTRAL DOMAIN GABOR FUSION	13
2.1	Mathematical Description of the conventional GD-OCM	13
2.2	Mathematical Description of Spectral Gabor Fusion	15
2.3	Experimental Verification	17
СНАРТ	ER Three: RESULTS AND DISCUSSION	21
3.1	Processing Speed Comparison	21
3.2	Fused Image Comparison	24
СНАРТ	ER Four: CONCLUSION	26
4.1	Conclusion	26
4.2	Reasearch Outcome	27
4.3	Future Direction	27
REFER	ENCES	29
A DDENI	DIV	21

LIST OF FIGURES

Figure 1-1 <i>In vivo</i> imaging of human finger skin taken by GD-OCM [24]7
Figure 1-2 Flow diagram of the imaging procedure of GD-OCM [27]8
Figure 1-3. Example of fusing algorithm of the GD-OCM [27]9
Figure 2-1 Comparison of flow diagrams of (left) the prior Gabor fusion and (right) the spectral
Gabor fusion methods
Figure 2-2 Examples of (a-e) acquired raw spectra at different focus position along the depth,
(f-j) filtered spectra, (k-o) filtered images correspond with each filtered spectra, (p) a fused
spectrum as a result of summation of all filtered spectra, and (q) the final fused image
obtained by performing the fast Fourier transform of the fused spectrum in (p). (BPF =
band-pass filter)
Figure 2-3 (a) and (b) are images obtained by a conventional FD-OCM and Spectral fusing
GD-OCM, respectively. (c) and (d) are examples of depth profile extracted from (a) and
(b), respectively19
Figure 3-1 Comparison plots of processing speed of the spectral domain Gabor fusion at
different spectrum sizes and different FFT size23
Figure 3-2 Comparison of three images obtained by (a) conventional FD-OCT, (b)
conventional GD-OCM, and (c) the proposed spectral fusing GD-OCM25

LIST OF TABLES

Table 1 Comparison the processing times of a conventional GD-fusion method	versus the
proposed method when the FFT size was fixed to 2048 points	21
Table 2 Comparison the processing times of a conventional GD-fusion method	versus the
proposed method when the FFT size was fixed to 4096 points	22
Table 3 Comparison the processing times of a conventional GD-fusion method	versus the
proposed method when the FFT size was kept the same with the spectrum size	e24

LIST OF ACRONYMS/ABBREVIATIONS

1D One Dimension

2D Two Dimensions

3D Three Dimensions

BW Bandwidth

DOF Depth of Focus

FD-OCT Frequency Domain Optical Coherence Tomography

FFT Fast Fourier Transform

FOV Field of View

FWHM Full-Width at Half-Maximum

GD-OCM Gabor Domain Optical Coherence Microscopy

NA Numerical Aperture

OCM Optical Coherence Microscopy

OCT Optical Coherence Tomography

CHAPTER One: INTRODUCTION

1.1 Introduction to the research problem and its significance

Even though skin canner, such as melanoma, can spread to other body parts quickly, it is also curable if detected early and treated properly. For most present day medical practitioners, the final cancer or pre-cancer diagnosis is based on the invasive technique of excisional or surgical biopsy that has been the only sure-way to determine if a growth is cancerous. While excisional biopsy is the proven standard method for cancer detection, many biopsies are done on a hit or miss basis because only small pieces of tissue are excised at random and dissected to check for cancerous cells.

A non-invasive, reliable and affordable cost imaging system with the capability of detecting early stage of pathology would be a valuable tool to use for screening or detecting pathology. In the quest for such a tool, photonics solutions have carried justified hopes within the last two decades. Optical coherence tomography (OCT) is one of emerging optical technologies that is capable of high resolution (i.e. in micrometers scale), high speed, and high sensitivity 3D imaging of living biological tissues. Nevertheless, the skin layer is as thin as 6 μ m and the skin cells size may vary from as small as 1 μ m to as large as 35 μ m, which set a requirement for axial and lateral resolutions of imaging system. Available commercial OCT systems are subject to limitation in resolution to about 10 μ m axially and ~20 μ m laterally, which is clearly not sufficient for resolving cellular structure in human skin.

Recently, a new technique of OCT imaging has been introduced called Gabor-domain optical coherence microscopy (GD-OCM), which combines high resolution microscope objective with dynamically refocus acquisition and Gabor-based data fusing to achieve invariant micron-class resolution (i.e. 2 µm) in 3D. However, the current implementation of Gabor-based acquisition and fusing involve large amount of acquired and processed data, prohibiting the use of this technology for quick diagnostics and real time applications. This project aims to address this limitation of GD-OCM by developing an alternative Gabor-based fusing algorithm that will dramatically improve the processing speed of the GD-OCM, allowing for quick imaging and diagnostics.

1.2 <u>Literature review</u>

Optical imaging technologies play an important role in medical diagnostics and treatments. Their main advantages are high resolution, high speed, and noninvasive capabilities. Optical coherence tomography (OCT) [1] is one of emerging optical imaging technologies that is capable of *in vivo* microscopic cross-sectional imaging of biological tissues and organs. By analogy to ultrasound imaging, yet at much higher resolution in 3D – of the order of the micron and possibly sub-micron, OCT is capable of non-invasive depth-resolved imaging of turbid media such as the human skin tissue [1]. OCT illuminates biological sample with broadband near infrared light beam and measured the amplitude and depth location of the backscattered light and uses it to construct a cross-sectional image that reveals structure beneath the sample surface. In most biological samples, the spatial variation of refractive index inside the sample causes variation in the amplitude

of the backscattered light reflected from inside biological tissues. Built on the coherence detection scheme such as Michelson or Mach-Zehnder interferometers, OCT is capable of measuring the small magnitude of this fluctuation down to the order of 10⁻⁶. OCT imaging can be performed by fixing a sample of interest in one arm of an interferometer, referred to as the sample arm, and placing a scanning mirror into the reference arm. The OCT system that acquired a sample depth profile by scanning the reference mirror is referred to as time domain OCT (TD-OCT) [1]. Combining with transverse scanning mechanism, 2D and 3D cross-sectional image of biological samples at microns resolution can be achieved.

The interference signal acquired by OCT is equivalent to an optical sampling of the sample reflectivity along the depth by using the low coherence of a broadband light source as a sampling gate [2]. Hence, the envelope of the temporal coherence serves as an axial point spread function (PSF). For a Gaussian spectral distribution assumption, the axial resolution Δz is given as $\Delta z = \frac{2\ln 2}{\pi} \left(\frac{\lambda_0^2}{\Delta \lambda}\right)$, where λ_0 is the source central wavelength, and Δz and $\Delta \lambda$ are the full width at half-maximum (FWHM) of the autocorrelation function and the power spectrum bandwidth of the light source, respectively [3, 4]. In addition to a broad spectral characteristic, an OCT light source should provide sufficient illumination power to penetrate deep inside the sample (typically 2 to 3 mm). Moreover, the center wavelength of the light source is usually selected to yield optimum absorption and backscattering that is between 800-1300 nm for biological samples [2, 4].

Separately, the lateral resolution is governed by a lateral PSF of an imaging lens in the sample arm. The lateral resolution can be estimated using the Rayleigh resolution criterion as

 $\Delta x = 1.22 \frac{\lambda_0}{NA}$, where NA is the numerical aperture of the objective lens [3]. The lateral resolution, therefore, can be improved by increasing the NA of the objective. Nevertheless, there is a trade-off between the lateral resolution and the depth of focus (DOF) since the lateral resolution is proportional to NA⁻¹, while the DOF is proportional to NA⁻². Therefore, the larger the NA of the objective lens the higher the lateral resolution but the smaller the DOF. As a result, typical OCT systems use low NA objectives to achieve sufficient DOF, e.g. ~2 mm in dense tissue, at the cost of low lateral resolution of often up to 20 μ m. Nevertheless, the skin layer is as thin as 6 μ m, which sets a requirement for depth resolution, and skin cells size may vary from as small as 1 μ m to as large as 35 μ m, which set a requirement for lateral resolution. Available commercial FD-OCT systems are subject to limitation in resolution to about 10 μ m axially and ~20 μ m laterally, which is clearly not sufficient for resolving cellular structure in human skin.

Furthermore, as a result of the large effort put forth by the scientific and industrial community to develop broader and broader source spectra, OCT has achieved (since the mid 1990s) remarkable axial resolution, starting in 1995 with mode-locked solid state lasers [5] and recently with supercontinuum sources [6, 7]. Therefore, an OCT extension that is capable of high lateral resolution to match the improved axial resolution is desirable. By using a higher NA objective in the sample arm (i.e. NA = 0.4), the first demonstration of high lateral resolution associated with the terminology of Optical Coherence Microscopy (OCM) emerged in 1994 [8].

Consequently, ultrahigh-resolution OCT was first demonstrated *in vivo* in 1999 with simultaneously up to \sim 1 μ m axial resolution in tissue and 3 μ m lateral resolution [9]. Nevertheless, the high lateral resolution achieved by simply opening the NA comes with the expense of a severe

reduction in DOF. To overcome the decrease in DOF that varies as the inverse square of the NA, the concept of dynamic focusing was introduced [10]. Since then, an open challenge has been to achieve high lateral resolution over a large imaging depth range as well as at sufficient speed capable for *in vivo* imaging, because it is only then that one can open a path for *in vivo* clinical applications seeking histology grade image quality.

Moreover, a recent advancement in Frequency Domain OCT (FD-OCT) allows depth-resolved imaging at high speed and high sensitivity attracting *in vivo* 3D and 4D (i.e. 3D imaging over time, of biological tissues) [11-13]. Based on coherence theory in the frequency domain [3], FD-OCT captures spectral interference at the output of an interferometer, e.g. Michelson interferometer, and then Fourier transform to obtain depth-resolved reflectivity profile along the incident beam path beneath the surface of the sample under test. The main advantage over the time domain counterpart is that FD-OCT obtained the whole depth profile at once without scanning of the optical path length of the reference beam. Hence its imaging speed is dramatically improved.

Most recently, a variant of OCT imaging was first introduced a team of scientists at the University of Rochester in 2008, Gabor-domain optical coherence microscopy (GD-OCM) [14], which uniquely combines the high speed imaging capability of the frequency domain OCT (FD-OCT) [15], the ability to dynamically refocus a liquid-lens-based dynamic focus microscope [16, 17], and a Gabor-based data fusing algorithm [18] to achieve invariant resolution of about 2 μ m in 3D across the volume of a sample, i.e. across a 2 mm × 2 mm × 2 mm field-of-view (FOV). Gabor fusion was also investigated in a Talbot band OCT system [19]. GD-OCM has been proven to be capable of cellular imaging of *in vivo* volumetric imaging of human skin [20]. Most recently,

the use of GD-OCM for 3D imaging at cellular resolution of normal and non-melanoma skins in comparison was reported [21], which shows the potential of GD-OCM to aid early diagnostics and guide removal of skin cancers. The potential of GD-OCM for characterization of human corneal layers and corneal diseases such as Fuchs dystrophy was also recently demonstrated [22].

Furthermore, utilizing a state-of-the-art broadband light source, the depth resolution of GD-OCM is about 2 µm in tissue. As a result, the GD-OCM technique offers enhanced resolution for cellular level skin imaging. The high resolution imaging at high speed with GD-OCM was achieved by a custom built high-speed high spectral-resolution spectrometer capable of up to 70,000 depth scans per second [23]. This high-speed imaging capability accommodated 3D *in vivo* imaging in biological samples, particularly in clinical trial stage. GD-OCM is capable of providing well defined structures of an *in vivo* human skin, where epidermis, dermis, sweat ducts, and, for the first time, basal layer cells in the dermal-epidermal junction were clearly observed (see Figure 1-1) [24].

The image acquisition of GD-OCM involves C-mode scanning adopted from an ultrasound imaging technique, in which multiple cross-sectional images are acquired corresponding with a discrete refocusing step along depth [25, 26]. The flow diagram of the GD-OCM system is illustrated in Figure 1-2. First, all system parameters were defined including exposure time of the CCD camera, number of spectra/frame, number of zones, and an applied voltage for each zone. The number of zone was determined by dividing the desire imaging depth range by the DOF. The applied voltages were determined from the measured relation between the applied voltage and the focal shift distance of the DF probe. The first voltage was then applied and the spectra were

acquired for a single frame. The process was then repeated for the next applied voltage until all zones were acquired. The data processing included DC subtraction and linear frequency calibration. Sequentially, the calibrated spectra were Fourier transformed yielding multiple intensity images illustrated in figure 3 (first column). A filtering window was calculated and then applied to each corresponding GD-sample as shown in the second column of figure 3. Finally, the filtered GD-samples were summed yielding the final image that contains mainly in-focus details for an entire cross-sectional area (figure 3).

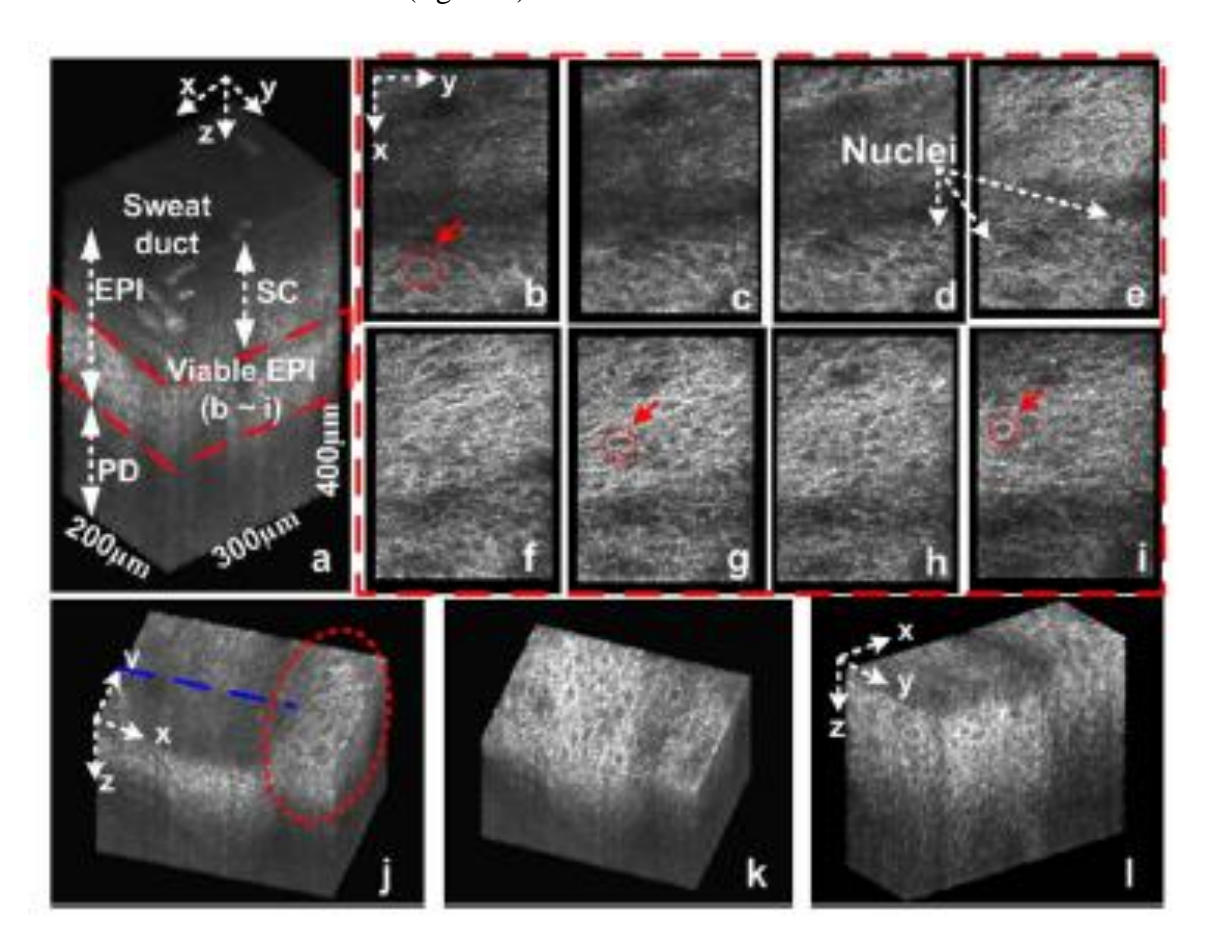


Figure 1-1 In vivo imaging of human finger skin taken by GD-OCM [24].

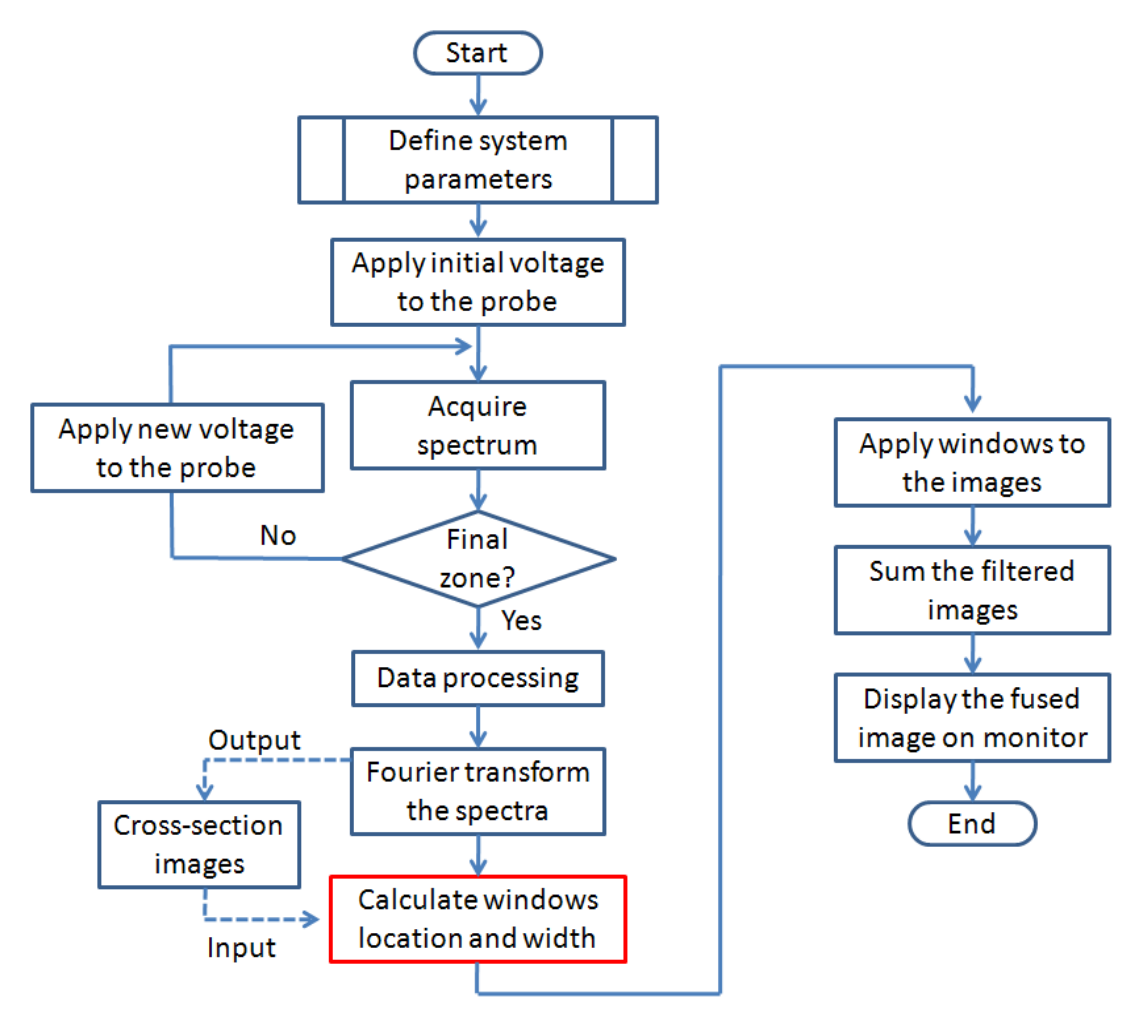


Figure 1-2 Flow diagram of the imaging procedure of GD-OCM [27].

Nevertheless, while GD-OCM is capable of 3D imaging of biological sample at invariant high resolution, allowing observation of cellular level of detail, superior than that obtained by commercially available OCT systems and other OCT extensions, it involved a massive amount of processing data (i.e. *5-10 times* more than a conventional FD-OCT processing). To be specific, for each single frame of GD-OCM image, it acquires five or more cross-sectional images, corresponding with different focus positions, and fused them together to obtain the final image

that contains only in-focus information as shown in Figure 1-3 [28]. The processing of a single set of 3D GD-OCM acquisition data could take up to 20,000,000 Fourier transformations of 4000 points per spectrum. This massive amount of Fourier transformation cause difficulty in pushing the GD-OCM technology for real time imaging and display that is essential for clinical use. This project aims to address this issue by investigating several approaches that will improved the processing speed of GD-OCM, involving both acquisition protocols and processing algorithms.

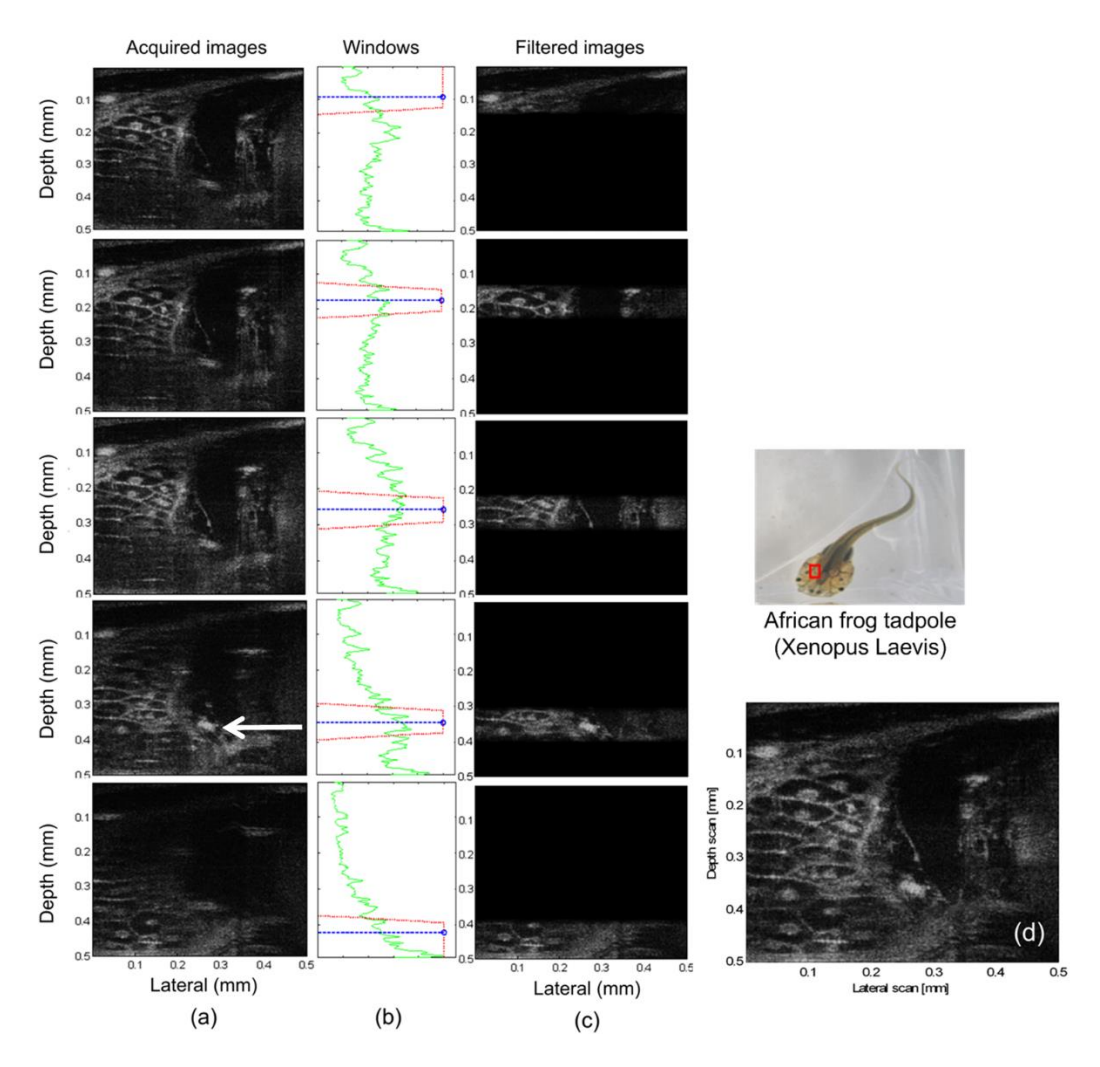


Figure 1-3. Example of fusing algorithm of the GD-OCM [27].

1.3 Research Objectives

- 1) To develop a new algorithm of GD-OCM processing that will dramatically improve the processing speed of the GD-OCM, i.e. cutting a processing time at least by half and allowing for real time processing and display.
- 2) To experimentally implement and verify the performance of the developed method.
- 3) To investigate applications of the developed method for tissues diagnostics.

1.4 Methodology

In conventional GD-OCM, the Gabor filtering and data fusing were done after Fourier transformation of all acquired spectra. As a result, the process involve huge amount of FFT, especially when performing 3D imaging, i.e. about 4-5 times more than conventional FD-OCT. This work flow prevents the original GD-OCM from fast processing and display. A main idea of this works is to investigate the possibility of performing Gabor filtering and fusing processes before performing FFT to obtain a final invariant high resolution image. For example, for 5-frames GD-OCM, all five set of spectral data need to be Fourier transform to get the final fused image and hence at least five times slower than a conventional FD-OCT. In contrary, with the new method all five data sets will be filtered and fused to become one fused spectrum and hence only one set of FFT is required to get the same fuse image. This will lead to a processing speed improvement of about five times as compared with the conventional method and would allow for real time processing of GD-OCM. The Gabor filtering that will be performed on the spectral data, i.e. before FFT, will be based on digital band-pass filter technique. The hypothesis is that the quality of the

final fused image will depend on the characteristics of the transmission window of the band-pass filter. Therefore, different type of band-pass filters will be investigated and compared their performance in order to choose only one type of filter for experimental implementation and validation. The project is divided into four stages as follow:

I) Development of a new algorithm for fast processing of GD-OCM

- Literature review on different techniques of digital filtering that can be applied for Gabor-based fusing algorithm of the GD-OCM.
- Develop mathematical models of the fusing algorithm based on different types of digital band-pass filters, such as Butterworth, Chebyshev, Bessel, and Equi-Ripple.
- Implement all potential algorithms in computer simulation using both Matlab and Labview programming to compare their theoretical performances, in terms of image resolution and contrast, processing speed, sensitivity, and robustness.
- Choose one or two algorithms that provide optimized performance to be experimentally verified.

II) Design and implement an experimental method based on the chosen algorithm.

- Design and built an imaging mechanics, such as laser beam scanning protocol, dynamic focusing scheme, and synchronization of data acquisition.
- Design a protocol for data acquisition to collect data that suits for each fusing algorithm.

- Implement the developed algorithm in Labview programming to interface with data acquisition. The image processing with Matlab may be also implemented if needed.
- Verify the synchronization between the data acquisition and digital signal processing systems to obtain optimized speed, resolution, and sensitivity.

III) Verify the performance of the implemented system.

- Perform 2D and 3D imaging of a phantom sample, a standard sample with known property,
 such as multilayer glass and/or resolution targets.
- Based on imaging performance of the phantom, modify the algorithm and system if needed.
- Perform in vivo imaging of various biological samples and analyze the performance of the system.
- Further modify the algorithm according to the imaging results of biological samples to further optimize the algorithm.

IV) Analyze an overall performance of the developed method and summarize the overall results.

The potential applications of the algorithm for biomedical diagnostics will be investigated.

CHAPTER Two: SPECTRAL DOMAIN GABOR FUSION

Despite its potential use for high resolution imaging over large 3D volumes, the current implementation of Gabor-based acquisition and fusion involve large amount of acquired and processed data that must be managed for real time applications. One solution that has been recently proposed and demonstrated leverages graphic processing units to boost the processing speed of the fast Fourier transformation [22]. Here, we present an approach to speed up the processing of GD-OCM datasets using a new algorithm for the GD-fusion in the spectral domain.

2.1 Mathematical Description of the conventional GD-OCM

In conventional FD-OCT, the Fourier transform of the detected spectral interference signal yields

$$I_{OCT}(z_D) = K \cdot \mathfrak{I}^{-1} \left\{ \hat{S}(k) \right\} * r_S(z_D) , \qquad (1)$$

where z_D is an optical path difference along the depth, K represents all other constant loss factors (e.g. power reflectivity and loss in reference arm, coupling loss, and fiber loss), $\hat{S}(k)$ is a power spectral density of the light source, the caret denotes a function in the spectral domain, and $r_S(z_D)$ denotes a sample reflectivity profile associated with the optical path difference, z_D .

Following the mathematical description of GD-OCM thoroughly derived in [18], any OCT or OCM image acquired using a NA microscope objective > 0.1 will be subjected to the Gabor filtering effect caused by its extremely short DOF. According to [18], the spectral interference

signal obtained by a system at different focus positions of the objective that has a narrow Gabor window (i.e. the DOF of the objective) may be expressed as

$$\hat{I}_{int}(k, m\delta z_D) = K\hat{S}(k) \int_{-\infty}^{\infty} g(z_D - m\delta z_D) \cdot r_S(z_D) \exp(ikz_D) dz_D, \tag{2}$$

where $m\delta z_D$ specifies an amount of shift of the focus position along the depth direction, $g(z_D - m\delta z_D)$ represents a normalized Gabor window caused by the DOF of the imaging optics. The integration term in Eq. (2) is in the form of a local Fourier transform or Gabor transform, where the DOF serves as a weighting window whose center may be shifted by varying the focal length of the dynamic focus probe. Following the mathematical derivation in [18], Fourier transformation of the spectral interference in (1) yields an OCT signal acquired at an arbitrary focal plane position that can be represented by

$$I_{OCT,m}(z_D) = K \Im^{-1} \{ \hat{S}(k) \} * r_S(z_D, m \delta z_D),$$
(3)

where $r_S(z_D, m\delta z_D)$ represents a backscattering event that occurs only within the DOF of the objective when the focal plane is shifted by an amount of $m\delta z_D$, which was referred to as a GD-sample in [18]. By utilizing the concept of the *inversion of the local Fourier transform* [29] and the Gabor's signal expansion [29], the final GD image can be reconstructed from multiple collected GD-samples by

$$I_{OCT}(z_D) = \sum_m g(z_D - m\delta z_D) \cdot \left[K \, \mathfrak{J}^{-1} \{ \hat{S}(k) \} * r_S(z_D, m\delta z_D) \right]. \tag{3}$$

The previous fusing algorithm of the GD-OCM [18] was based on this Eq. (3), which reconstructs an invariant high resolution depth profile of the sample by acquiring multiple cross-sectional images at different focal planes along the depth, multiplying each image with a corresponded

sliding window, and combining all filtered images to form a final GD-OCM image. We refer to this fusing method as "spatial-domain GD-fusion".

2.2 <u>Mathematical Description of Spectral Gabor Fusion</u>

In this paper however, aiming to optimize the processing speed of the Gabor fusion method, we investigated an alternative interpretation of Eq. (3). By inverse Fourier transform Eq. (3) back to the spectral domain and using the Fourier transform pair relation between Eq. (1) and (2), we obtain a spectral interference signal corresponding to the combined GD-samples as

$$\hat{I}_{int}(k) = \sum_{m} \mathfrak{I}^{-1} \{ g(z_D - m\delta z_D) \} * \hat{I}_{int}(k, m\delta z_D).$$
 (4)

Eq. (4) reveals that the GD-fusion can also be performed in the spectral domain by convoluting some appropriate sliding spectral Gabor windows, i.e. $\Im^{-1}\{g(z_D - m\delta z_D)\}$, with each spectral interference signal acquired at different focus positions of the objective lens.

In practice, the convolution term in Eq. (4) is equivalent to performing a band-pass filter on a spectral interference signal [30]. The filtered spectral interference signals are then summed to form a final fused spectral interference signal that contains only in-focus signal from each acquired raw spectrum. Finally, by Fourier transform of the final fused spectra, a cross sectional image that contains in-focus detail across the desired imaging depth similar to that achieved in [18] can be obtained. We refer to this fusing method as "spectral-domain GD-fusion". The new fusing method is expected to improve the processing speed of the GD-OCM since only one Fourier transformation

per one depth scan is required as oppose to multiple Fourier transformation per one depth scan in the original GD-OCM. Figure 2-1 shows comparison of the flow diagram of the spectral fusion method as compared with the original approach in [18].

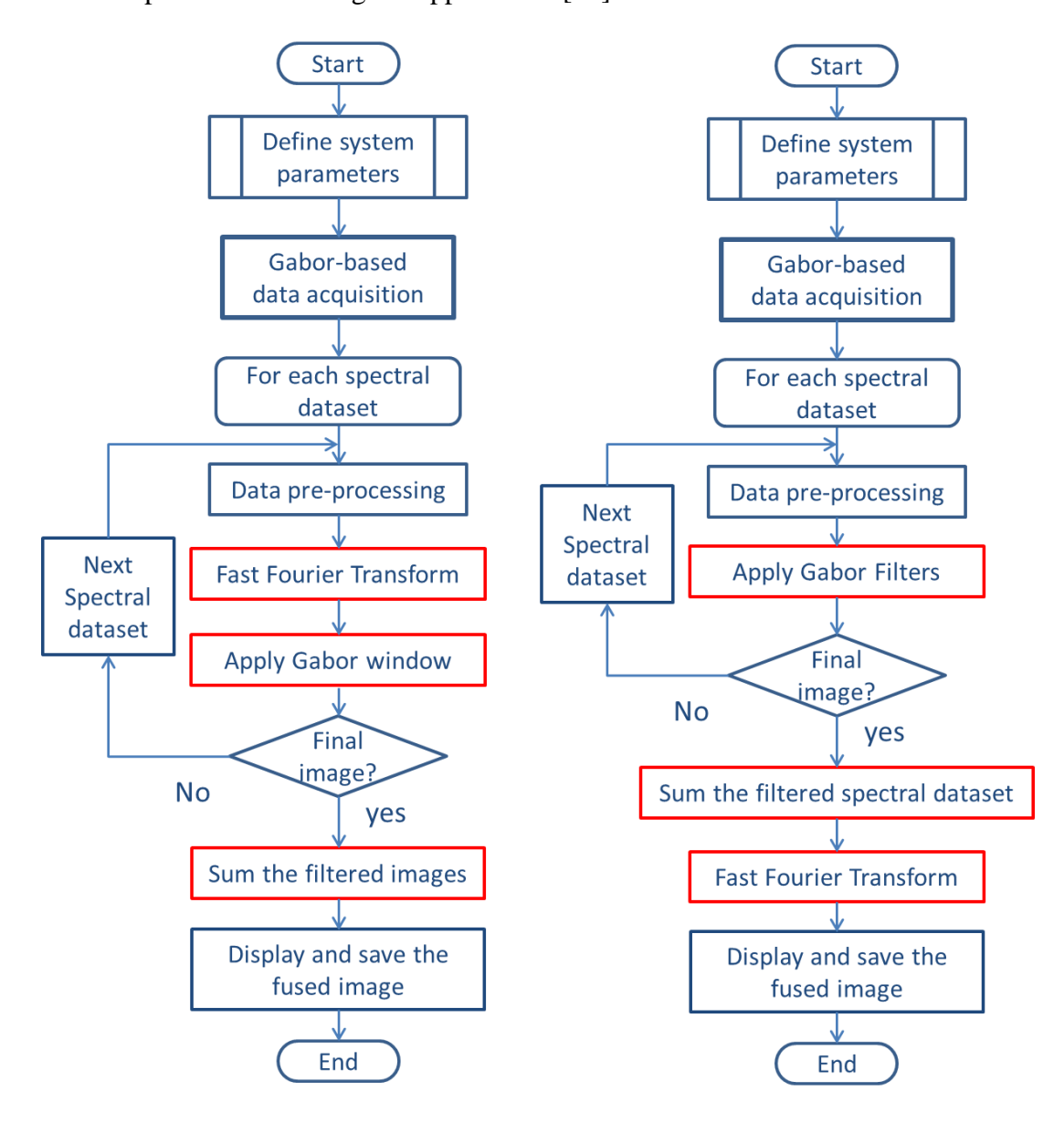


Figure 2-1 Comparison of flow diagrams of (left) the prior Gabor fusion and (right) the spectral Gabor fusion methods.

2.3 Experimental Verification

To experimentally verify the speed improvement, the new spectral fusing method and the prior spatial fusing method were implemented in LabVIEW programming environment (National Instrument, USA) by following the flow charts shown in Fig. 1. The processing host was a desktop computer with Intel Core i5, 3.1 GHz CPU, 16 GB memory, and under 64 bits operating system running Window 7 Professional. From Fig. 1, since there is no difference in data acquisition for both methods, only processing times were compared and presented. Therefore, a set of GD-OCM data that was pre-acquired and stored in the computer's hard drive was used for the study. The number of GD-samples was 5 images that were acquired at every 100 microns focal shift interval along depth. Each GD sample consisted of 1000 spectra per frame. Each spectrum was acquired at a sampling resolution of 3600 points per spectrum. To compare the performance of both methods for different sizes of spectra, the acquired spectra were then down sampled to the sizes of 500, 1000, 1500, 2000, 2500, 3000, and 3500 points per spectrum as shown in **Error! Reference source** not found. All processes were kept the same between the two methods except those in the red box shown in Fig. 1, which are the fusion process and the fast Fourier transform (FFT). In each table, the FFT size was kept the same for both methods for a given spectrum size.

The implementation of the spatial-domain GD-fusion followed the same procedure as presented in [18]. While we previously showed that the spatial-domain GD-fusion is capable of adaptive filtering for different types of samples, here we will assume the same type of samples in comparing the two approaches, and as such in both cases pre-optimized filters will be considered. Therefore, the fusing process of the spatial-domain GD-fusion involves multiplication of each

acquired image with a corresponding pre-optimized Gabor window and summation of all filtered images to obtain the final fused image. On the other hand, the spectral-domain GD-fusion involves application of each acquired spectrum with a pre-optimized band-pass filter and summation of all filtered spectra to obtain the final fused spectrum. The final fused image was obtained by Fourier transformation of the fused spectra.

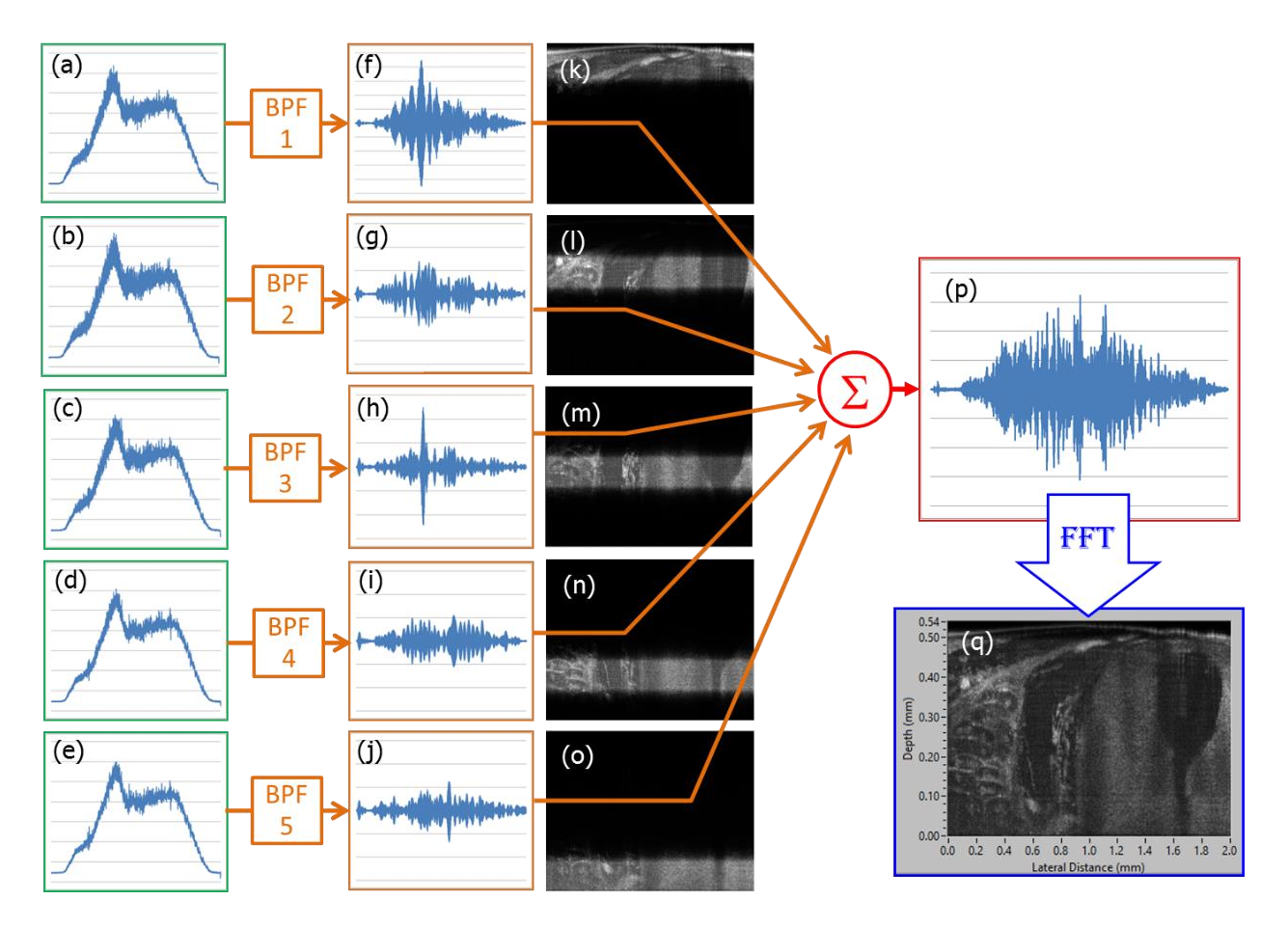


Figure 2-2 Examples of (a-e) acquired raw spectra at different focus position along the depth, (f-j) filtered spectra, (k-o) filtered images correspond with each filtered spectra, (p) a fused spectrum as a result of summation of all filtered spectra, and (q) the final fused image obtained by performing the fast Fourier transform of the fused spectrum in (p). (BPF = band-pass filter)

Figure 2-2 illustrates the process of the spectral-domain GD-fusion. Figure 2-2 (a-e) are examples of the raw spectra acquired at different focus position inside the sample. In this demonstration, a Chebyshev digital band-pass filter was implemented for the spectral filtering [30]. Figure 2-2 (f-j) shows example of the filtered spectra. As for verification of the filtering process, Figure 2-2 (k-o) demonstrates their corresponded cross-sectional images obtained by FFT of each frame of the filtered spectra. Figure 2-2 (p) is an example of a combined (or spectrally fused) spectrum. Figure 2-2 (q) shows the final fused image obtained from the FFT of a frame of fused spectra. It should also be pointed out that the spectral fusing method also provides DC removal in the process, which is a necessary pre-processing step for the spatial-domain fusion.

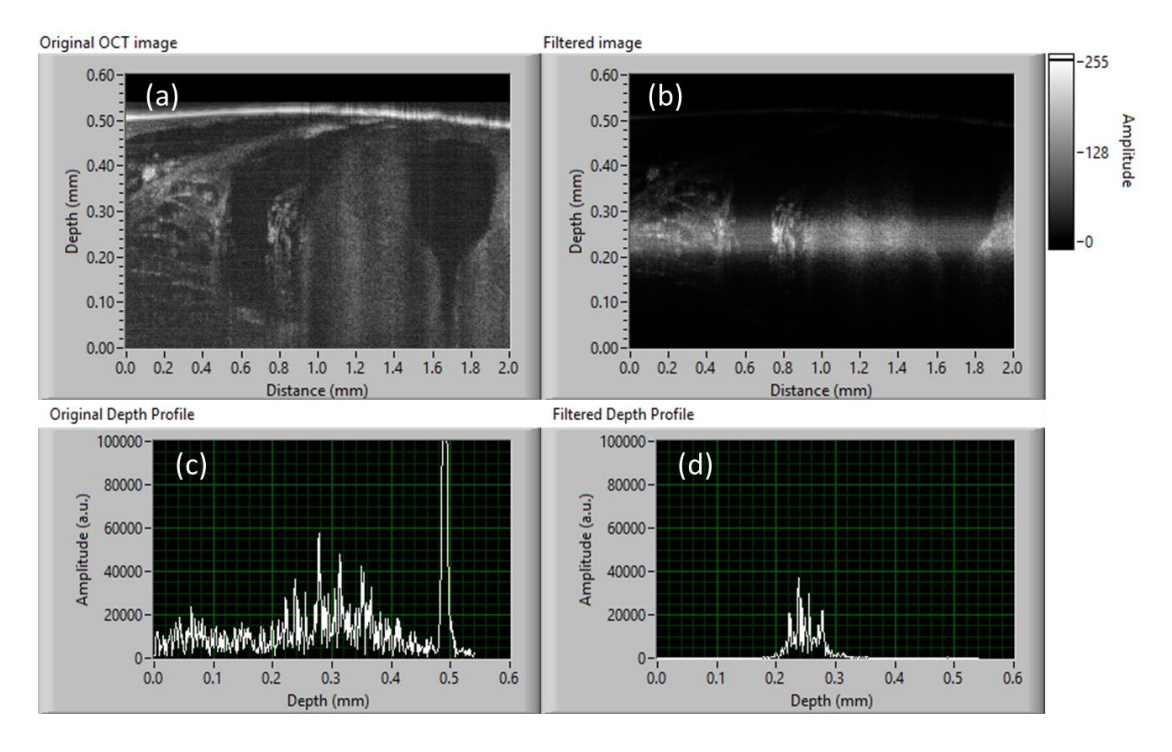


Figure 2-3 (a) and (b) are images obtained by a conventional FD-OCM and Spectral fusing GD-OCM, respectively. (c) and (d) are examples of depth profile extracted from (a) and (b), respectively.

Figure 2-3 (a) and (b) show a comparison of cross-sectional images acquired by a conventional FD-OCM and the spectral fusing GD-OCM, respectively. Figure 2-3 (a) and (b) are comparison of depth profiles extracted at around 0.2 mm lateral position of Figure 2-3 (a) and (b), respectively. The original FD-OCM image contains both in-focus and out out-of-focus information as shown in Figure 2-3 (a). The spectral fusing method can filter out out-of-focus information and left only in-focus information by properly choosing the filter as shown in Figure 2-3 (b).

CHAPTER Three: RESULTS AND DISCUSSION

3.1 Processing Speed Comparison

Processing times of both methods, starting from the data pre-processing until display the fused image, were measured and compared for the case of 2048 and 4096 FFT sizes as shown in **Error! Reference source not found.** and Table 2, respectively. Moreover, Table 3 shows the processing times of a conventional GD-fusion of different sizes of acquired spectra as compared with the processing time of the proposed method when the FFT sizes were the same with spectrum sizes. The comparison was performed for different spectral lengths, ranging from 500 to 3500 points per spectrum. Each processing time in all tables is presented as mean \pm standard deviation (S.D.) computed from 10 measurements (N =10) for each case.

Table 1 Comparison the processing times of a conventional GD-fusion method versus the proposed method when the FFT size was fixed to 2048 points

Spectrum size	FFT size	Total processing time (ms)	
(pixels)	(points)	Conventional GD-fusion	Proposed GD-fusion
500	2048	202.0 ± 0.7	86.9 ± 1.3
1000	2048	214.3 ± 1.1	131.6 ± 1.3
1500	2048	227.4 ± 1.0	177.0 ± 1.2
2000	2048	239.0 ± 0.9	219.3 ± 0.8
2500	2048	242.1 ± 0.9	264.6 ± 1.9
3000	2048	255.5 ± 1.2	308.6 ± 2.1
3500	2048	272.8 ± 1.4	358.5 ± 2.1

Table 2 Comparison the processing times of a conventional GD-fusion method versus the proposed method when the FFT size was fixed to 4096 points

Spectrum size	FFT size	Total processing time (ms)	
(pixels)	(points)	Conventional GD-fusion	Proposed GD-fusion
500	4096	383.3 ± 0.8	120.6 ± 1.3
1000	4096	398.5 ± 1.7	165.3 ± 1.2
1500	4096	410.5 ± 2.1	209.7 ± 1.1
2000	4096	425.0 ± 2.4	254.3 ± 1.3
2500	4096	437.9 ± 2.9	300.1 ± 1.5
3000	4096	448.7 ± 0.9	344.7 ± 2.7
3500	4096	467.6 ± 1.4	395.2 ± 1.8

The result shows that, in the cases of fixed 4096 point FFT, the new fusing algorithm outperforms the conventional method. Especially when the spectrum size was small (e.g. 500 points spectrum), the processing time of the proposed method is about three times faster than that of the conventional method. This scenario can be occurred when high axial resolution is demanded (i.e. requires dense sampling in FFT) but only shallow depth (e.g. less than 1 mm) information is available or off interest and hence small number of sampling points of an acquired spectrum is sufficient (i.e. reflection from shallow depth causes low modulation frequency on the spectral interference). For instance, imaging with 1 µm axial point spread function (PSF) over 1 mm imaging depth will require at least 2000 point of depth sampling and hence will require 4096 points FFT.

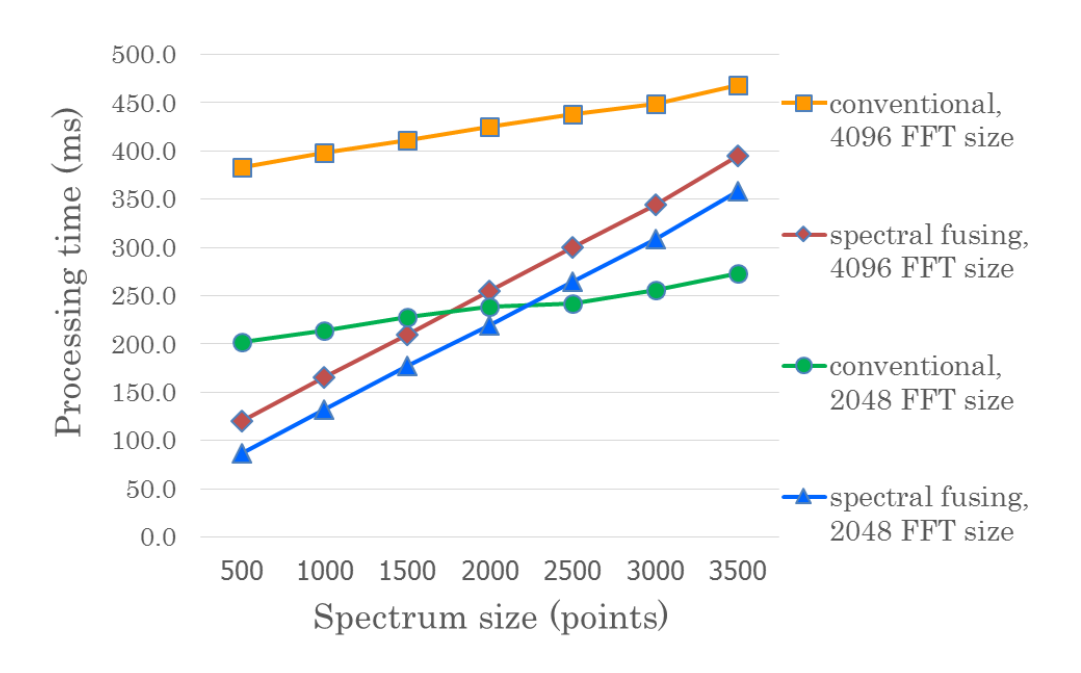


Figure 3-1 Comparison plots of processing speed of the spectral domain Gabor fusion at different spectrum sizes and different FFT size.

Nevertheless, the band-pass filtering took more time to process when the spectrum size is large and hence the overall processing time can be longer than that of the conventional fusing, such as in the case of 3500 points spectrum and 2048 points FFT. This scenario can be occurred when performing deep imaging, (e.g. 2-5 mm) at low axial resolution, which requires a fine sampling of acquired spectra but small size FFT. For example, when imaging over 4 mm depth with 10 µm axial PSF, at least 800 points of depth sampling is demanded. In the cases of when the FFT size is the same with spectrum, the processing speed of both conventional fusing and the proposed spectral fusing methods are almost the same with the new method is slightly faster as shown in Table 3.

Table 3 Comparison the processing times of a conventional GD-fusion method versus the proposed method when the FFT size was kept the same with the spectrum size.

Spectrum size	FFT size	Total processing time (ms)	
(pixels)	(points)	Conventional GD-fusion	Proposed GD-fusion
500	500	68.3 ± 0.7	63.3 ± 1.2
1000	1000	121.2 ± 0.8	115.1 ± 0.9
1500	1500	181.4 ± 1.0	171.8 ± 1.2
2000	2000	232.2 ± 0.8	221.1 ± 1.0
2500	2500	301.7 ± 2.2	276.7 ± 1.3
3000	3000	348.6 ± 2.2	329.9 ± 2.1
3500	3500	430.7 ± 2.5	387.5 ± 2.0

3.2 Fused Image Comparison

Figure 3-2 shows a comparison of three images, representing (a) a conventional FD-OCT image, (b) a conventional GD-image obtained by using an algorithm presented in [5], and (c) a GD-image obtained by using our proposed spectral fusing method. The fused images from both the spatial domain GD-fusion (Figure 3-2(b)) and the spectral domain GD-fusion (Figure 3-2(c)) shows similar resolution and contrast that are quasi-invariant over depth as compared with the cross-sectional image obtain by the conventional GD-COM in Figure 3-2(a).

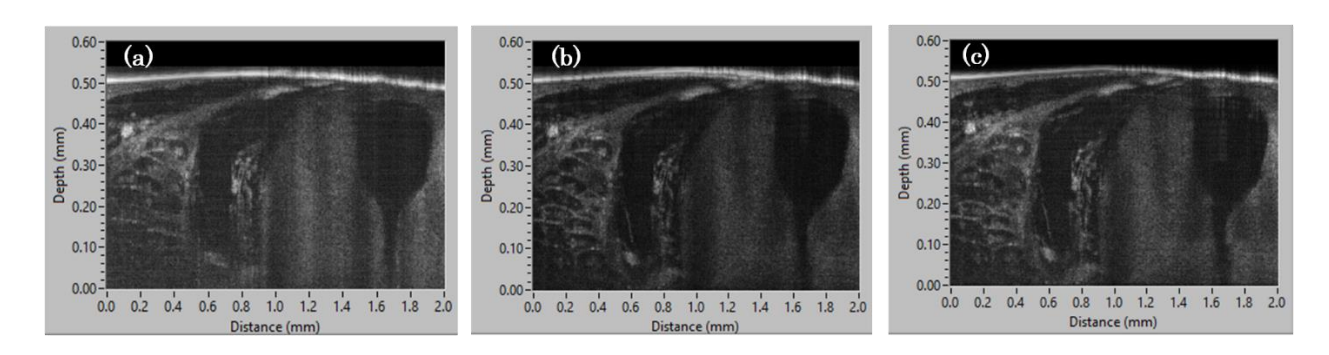


Figure 3-2 Comparison of three images obtained by (a) conventional FD-OCT, (b) conventional GD-OCM, and (c) the proposed spectral fusing GD-OCM.

CHAPTER Four: CONCLUSION

4.1 Conclusion

Gabor-domain optical coherence microscopy (GD-OCM) is one of many variations of optical coherence tomography (OCT) techniques that aims for invariant high resolution across a three dimensional field of view, by utilizing the ability to dynamically refocus the imaging optics in the sample arm. GD-OCM acquires multiple cross-sectional images at different focus positions of the objective lens and then fuses them to obtain invariant high resolution 3D image of the sample, which comes with the intrinsic drawback of a longer processing time as compared to conventional Fourier domain OCT.

Here, we have developed an alternative Gabor fusing algorithm, the spectral-fusion technique, that directly processes each acquired spectrum and combining them prior to the Fourier transformation to obtain a depth profile. The new fusing algorithm was implemented and its performance was compared to that of the prior GD-OCM spatial-fusion approach. The spectral-fusion approach shows twice the speed of the spatial-fusion approach for a spectrum size of less than 2000 point sampling, which is a commonly used spectrum size in OCT imaging, including GD-OCM.

In conclusion, we presented a spectral fusing technique for GD-OCM that is based on Gabor filtering and fusion in the spectral domain. The proposed technique shows improved speed for high definition sampling in the spatial domain compared to the spatial-fusion technique. In addition, it should also be pointed out that the spectral fusing method also provides DC removal

in the process, which is a necessary pre-processing step for the conventional method. To date, a commonly used spectrum size in our GD-OCM imaging system is about 1000 points per spectrum, processed with a 4096 points FFT, which is largely sufficient for imaging across the depth of 1 mm at equivalent 0.5 µm sampling of a 2 µm axial PSF, and equivalently 1 µm sampling for a 2048 points FFT. In both cases, the spectral-domain fusion is about twice as fast as the spatial-domain fusion. Furthermore, it is worth noting that a hardware implementation of the processing algorithm is possible by utilizing hardware-based signal processing, such as an FPGA enabled frame grabber [31] or other similar acquisition devices. The hardware-based filtering is expected to greatly improve the processing speed of the presented spectral fusing method, which will be further investigated in the future.

4.2 Reasearch Outcome

- 1) A new fusing technique for GD-OCM was developed.
- 2) A manuscript was submitted and under peer reviewed to be published in the Optics Letters journal (2014 impact factor = 3.292).

4.3 Future Direction

1) Further improve the processing speed of the spectral domain GD fusion by investigating the use of FPGA equipped frame grabber. The main idea is to push all spectral processing, including the spectral filtering and fusing into the acquisition device. The proposed method will

greatly reduce the processing time of the overall system and has potential to help moving forward the technology of GD-OCM one step closer to real time diagnostics and applications.

- 2) Experimentally verify the FPGA-based spectral fusing GD-OCM and investigate its capability for high speed GD-OCM imaging.
- 3) Investigate the use of the developed prototype for high speed high resolution imaging of biological samples, skin imaging, and material characterization.

REFERENCES

- 1. D. Huang, E. A. Swanson, C. P. Lin, J. S. Schuman, W. G. Stinson, W. Chang, M. R. Hee, T. Flotte, K. Gregory, C. A. Puliafito, and J. G. Fujimoto, "Optical coherence tomography," Science **254**, 1178-1181 (1991).
- 2. A. F. Fercher, W. Drexler, C. K. Hitzenberger, and T. Lasser, "Optical coherence tomography-principles and applications," Reports on progress in physics **66**, 239-303 (2003).
- 3. M. Born and E. Wolf, *Principles of Optics, seventh expanded edition*, Cambridge, England (Cambridge University Press, 1999).
- 4. B. E. Bouma and G. J. Tearney, *Handbook of optical coherence tomography* (Marcel Dekker, Inc., 2002).
- 5. B. Bouma, G. J. Tearney, S. A. Boppart, M. R. Hee, M. E. Brezinski, and J. G. Fujimoto, "High-resolution optical coherence tomographic imaging using a mode-locked Ti: Al2O3 laser source," Optics Letters **20**, 1486-1488 (1995).
- 6. A. Aguirre, N. Nishizawa, J. Fujimoto, W. Seitz, M. Lederer, and D. Kopf, "Continuum generation in a novel photonic crystal fiber for ultrahigh resolution optical coherence tomography at 800 nm and 1300 nm," Optics Express **14**, 1145-1160 (2006).
- 7. P. Cimalla, J. Walther, M. Mehner, M. Cuevas, and E. Koch, "Simultaneous dual-band optical coherence tomography in the spectral domain for high resolution in vivo imaging," Opt. Express 17, 19486-19500 (2009).
- 8. J. A. Izatt, M. R. Hee, G. M. Owen, E. A. Swanson, and J. G. Fujimoto, "Optical coherence microscopy in scattering media," Optics Letters **19**, 590-592 (1994).
- 9. W. Drexler, U. Morgner, F. X. K'rtner, C. Pitris, S. A. Boppart, X. D. Li, E. P. Ippen, and J. G. Fujimoto, "In vivo ultrahigh-resolution optical coherence tomography," Optics Letters **24**, 1221-1223 (1999).
- 10. J. M. Schmitt, S. L. Lee, and K. M. Yung, "An optical coherence microscope with enhanced resolving power in thick tissue," Optics Communications **142**, 203-207 (1997).
- 11. A. F. Fercher, C. K. Hitzenberger, G. Kamp, and S. Y. El-Zaiat, "Measurement of intraocular distances by backscattering spectral interferometry," Opt. Comm. **117**, 43-48 (1995).
- 12. M. Choma, M. Sarunic, C. Yang, and J. Izatt, "Sensitivity advantage of swept source and Fourier domain optical coherence tomography," Optics Express 11, 2183-2189 (2003).
- 13. J. F. De Boer, B. Cense, B. H. Park, M. C. Pierce, G. J. Tearney, and B. E. Bouma, "Improved signal-to-noise ratio in spectral-domain compared with time-domain optical coherence tomography," Optics Letters **28**, 2067-2069 (2003).
- 14. J. P. Rolland, P. Meemon, S. Murali, A. Jain, N. Papp, K. P. Thompson, and K. S. Lee, "Gabor domain optical coherence microscopy," in *1st Canterbury Workshop on Optical Coherence Tomography and Adaptive Optics* (Proceeding of SPIE, 2008), 71390F.
- 15. A. F. Fercher, C. K. Hitzenberger, G. Kamp, and S. Y. El-Zaiat, "Measurement of intraocular distances by backscattering spectral interferometry," Optics Communications **117**, 43-48 (1995).

- 16. S. Murali, K. S. Lee, and J. P. Rolland, "Invariant resolution dynamic focus OCM based on liquid crystal lens," Optics Express **15**, 15854-15862 (2007).
- 17. S. Murali, K. Thompson, and J. Rolland, "Three-dimensional adaptive microscopy using embedded liquid lens," Optics Letters **34**, 145-147 (2009).
- 18. J. P. Rolland, P. Meemon, S. Murali, K. P. Thompson, and K. S. Lee, "Gabor-based fusion technique for Optical Coherence Microscopy," Optics Express 18, 3632-3642 (2010).
- 19. P. Bouchal, A. Bradu, and A. G. Podoleanu, "Gabor fusion technique in a Talbot bands optical coherence tomography system," Optics express **20**, 5368-5383 (2012).
- 20. K. S. Lee, K. P. Thompson, P. Meemon, and J. P. Rolland, "Cellular resolution optical coherence microscopy with high acquisition speed for in-vivo human skin volumetric imaging," Optics letters **36**, 2221-2223 (2011).
- 21. K.-S. Lee, H. Zhao, S. F. Ibrahim, N. Meemon, L. Khoudeir, and J. P. Rolland, "Three-dimensional imaging of normal skin and nonmelanoma skin cancer with cellular resolution using Gabor domain optical coherence microscopy," Journal of biomedical optics **17**, 126006-126006 (2012).
- 22. P. Tankam, Z. He, Y.-J. Chu, J. Won, C. Canavesi, T. Lepine, H. B. Hindman, D. J. Topham, P. Gain, and G. Thuret, "Assessing microstructures of the cornea with Gabor-domain optical coherence microscopy: pathway for corneal physiology and diseases," Optics letters **40**, 1113-1116 (2015).
- 23. K. S. Lee, K. P. Thompson, and J. P. Rolland, "Broadband astigmatism-corrected Czerny—Turner spectrometer," Opt. Express **18**, 23378-23384 (2010).
- 24. K. S. Lee, K. P. Thompson, P. Meemon, and J. P. Rolland, "Cellular resolution optical coherence microscopy with high acquisition speed for in-vivo human skin volumetric imaging," Opt. Lett. **36**, 2221-2223 (2011).
- 25. M. D. Sherar, M. B. Noss, and F. S. Foster, "Ultrasound backscatter microscopy images the internal structure of living tumor spheroids," Nature **330**, 493-495 (1987).
- 26. R. Huber, M. Wojtkowski, J. G. Fujimoto, J. Y. Jiang, and A. E. Cable, "Three-dimensional and C-mode OCT imaging with a compact, frequency swept laser source at 1300 nm," Optics Express **13**, 10523-10538 (2005).
- 27. P. Meemon, "Development of Optical Coherence Tomography for Tissue Diagnostics," Dissertation (University of Central Florida, Orlando, 2010).
- 28. J. P. Rolland, P. Meemon, S. Murali, K. P. Thompson, and K. S. Lee, "Gabor-based fusion technique for Optical Coherence Microscopy," Opt. Express 18, 3632-3642 (2010).
- 29. H. H. Barrett and K. Myers, *Foundations of image science. Hoboken* (NJ: John Wiley & Sons, 2004).
- 30. J. V. D. Vegte, Fundamentals of Digital Signal Processing with Cdrom (Prentice Hall PTR, 2001).
- 31. T. E. Ustun, N. V. Iftimia, R. D. Ferguson, and D. X. Hammer, "Real-time processing for Fourier domain optical coherence tomography using a field programmable gate array," Review of Scientific Instruments **79**, 114301 (2008).

APPENDIX

Spectral fusing Gabor domain optical coherence microscopy

PANOMSAK MEEMON, 1,2,* JOEWONO WIDJAJA, 1 JANNICK P. ROLLAND 2

- ¹ School of Physics, Institute of Science, Suranaree University of Technology, Thailand 30000
- ² The Institute of Optics, University of Rochester, New York, USA 14627
- *Corresponding author: panomsak@sut.ac.th

Received XX Month XXXX; revised XX Month, XXXX; accepted XX Month XXXX; posted XX Month XXXX (Doc. ID XXXXX); published XX Month XXXX

Gabor-domain optical coherence microscopy (GD-OCM) is one of many variations of optical coherence tomography (OCT) techniques that aims for invariant high resolution across a three dimensional field of view, by utilizing the ability to dynamically refocus the imaging optics in the sample arm. GD-OCM acquires multiple cross-sectional images at different focus positions of the objective lens and then fuses them to obtain invariant high resolution 3D image of the sample, which comes with the intrinsic drawback of a longer processing time as compared to conventional Fourier domain OCT. Here, we report on an alternative Gabor fusing algorithm, the spectral-fusion technique, that directly processes each acquired spectrum and combining them prior to the Fourier transformation to obtain a depth profile. The implementation of the new fusing algorithm is presented and its performance is compared to that of the prior GDspatial-fusion approach. The spectral-fusion approach shows twice the speed of the spatial-fusion approach for a spectrum size of less than 2000 point sampling, which is a commonly used spectrum size in OCT imaging, including GD-OCM. © 2015 Optical Society of

OCIS codes: (100.3010) Image reconstruction techniques; (110.0180) Microscopy; (110.1085) Adaptive imaging; (110.4500) Optical coherence tomography.

http://dx.doi.org/10.1364/OL.99.099999

Optical imaging technologies play an important role in medical diagnostics and treatments. Their main advantages are high resolution, high speed, and noninvasive capabilities. Optical coherence tomography (OCT) [1] is one of emerging optical imaging technologies that is capable of *in vivo* microscopic cross-sectional imaging of biological tissues and organs. Particularly, one outstanding capability of OCT is the ability to provide depth-section of the sample at high resolution and sensitivity. Beside high speed and functional imaging capability, another key parameter that will open path for optical diagnostics using OCT technology is high resolution imaging (i.e. in a

regime of a few microns or sub-micron), particularly in three dimensions (3D).

Even though the lateral resolution of OCT can be independently improved by opening the numerical aperture (NA) of the imaging optics, the high lateral resolution is normally maintained only over a short range as limited by the depth of focus (DOF) that varies inversely and quadratically with NA. To achieve quasi-invariant lateral resolution over an imaging depth range of \sim 2-3 mm, which corresponds with the depth penetration limit of OCT imaging, conventional OCT utilizes low NA imaging optics (e.g. NA < 0.1) that provides quasi-invariant lateral resolution in the range of 10 to 30 μm . By using a higher NA objective in the sample arm (i.e. NA = 0.4), the first demonstration of high lateral resolution associated with the terminology of Optical Coherence Microscopy (OCM) emerged in 1994 [2]. Consequently, in vivo cellular imaging of biological sample with lateral resolution down to 3 μm was demonstrated [3, 4]. Nevertheless, the high lateral resolution achieved by simply opening the NA comes at the expense of a severe reduction in the DOF [4]. To overcome the decrease in DOF that varies as the inverse square of the NA, a combination of OCM imaging and a dynamic focusing scheme was demonstrated [5, 6].

Furthermore, a variant of OCT imaging was first introduced in 2008, Gabor-domain optical coherence microscopy (GD-OCM) [7], which uniquely combines the high speed imaging capability of the frequency domain OCT (FD-OCT) [8], the ability to dynamically refocus a liquidlens-based dynamic focus microscope [9, 10], and a Gabor-based data fusing algorithm [11] to achieve invariant resolution of about 2 µm in 3D across the volume of a sample, i.e. across a $2 \text{ mm} \times 2 \text{ mm} \times 2 \text{ mm}$ field-of-view (FOV). Gabor fusion was also investigated in a Talbot band OCT system [12]. GD-OCM has been proven to be capable of cellular imaging of in vivo volumetric imaging of human skin [13]. Most recently, the use of GD-OCM for 3D imaging at cellular resolution of normal and non-melanoma skins in comparison was reported [14], which shows the potential of GD-OCM to aid early diagnostics and guide removal of skin cancers. The potential of GD-OCM for characterization of human corneal layers and corneal diseases such as Fuchs dystrophy was also recently demonstrated [15].

Despite its potential use for high resolution imaging over large 3D volumes, the current implementation of Gabor-based acquisition and fusion involve large amount of acquired and processed data that must be managed for real time applications. One solution that has been recently proposed and demonstrated leverages graphic processing units to boost the processing speed of the fast Fourier transformation

[16]. Here, we present an approach to speed up the processing of GD-OCM datasets using a new algorithm for the GD-fusion in the spectral domain.

Following the mathematical description of GD-OCM thoroughly derived in [11], any OCT or OCM image acquired using a NA microscope objective > 0.1 will be subjected to the Gabor filtering effect caused by its extremely short DOF. According to [11], the spectral interference signal obtained by a system at different focus positions of the objective that has a narrow Gabor window (i.e. the DOF of the objective) may be expressed as

$$\hat{I}_{int}(k,m) = K\hat{S}(k) \int_{-\infty}^{\infty} g(z_D - m\delta z_D) \cdot r_S(z_D) \exp(ikz_D) dz_D,$$
(1)

where the caret denotes a function in the spectral domain, z_D is an optical path difference along the depth, $m\delta z_D$ specifies an amount of shift of the focus position along the depth direction, $g(z_D-m\delta z_D)$ represents a normalized Gabor window caused by the DOF of the imaging optics, K represents all other constant loss factors (e.g. power reflectivity and loss in reference arm, coupling loss, and fiber loss), $\hat{S}(k)$ is a power spectral density of the light source, and $r_S(z_D)$ denotes a sample reflectivity profile associated with the optical path difference, z_D . Eq. (1) states that the obtained spectral interference signal is a multiplication between the source spectrum and the integral term that is associated with light reflection at multiple depths from the sample. Following the mathematical derivation in [11], Fourier transformation of the spectral interference in (1) yields an OCT signal acquired at an arbitrary focal plane position that can be represented by

$$I_{OCT,m}(z_D) = K \mathfrak{F}^{-1} \{\widehat{S}(k)\} * r_S(z_D, m \delta z_D)$$
 (2)

where $r_S(z_D, m\delta z_D)$ represents a backscattering event that occurs only within the DOF of the objective when the focal plane is shifted by an amount of $m\delta z_D$, which was refered to as a *GD-sample* in [11]. By utilizing the concept of the *inversion of the local Fourier transform* and the *Gabor's signal expansion*, the final GD image can be reconstructed from multiple collected GD-samples by

$$I_{OCT}(z_D) = \sum_m g(z_D - m\delta z_D) \cdot \left[K \, \mathfrak{F}^{-1} \left\{ \widehat{\mathfrak{S}}(k) \right\} * r_S(z_D, m\delta z_D) \right]. \tag{3}$$

The previous fusing algorithm of the GD-OCM [11] was based on this Eq. (3), which reconstructs an invariant high resolution depth profile of the sample by acquiring multiple cross-sectional images at different focal planes along the depth, multiplying each image with a corresponded sliding window, and combining all filtered images to form a final GD-OCM image. We refer to this fusing method as "spatial-domain GD-fusion".

In this paper however, aiming to optimize the processing speed of the Gabor fusion method, we investigated an alternative interpretation of Eq. (3). By inverse Fourier transform Eq. (3) back to the spectral domain and using the Fourier transform pair relation between Eq. (1) and (2), we obtain a spectral interference signal corresponding to the combined GD-samples as

$$\hat{I}_{int}(k) = \sum_{m} \mathfrak{F}^{-1} \{ g(z_D - m\delta z_D) \} * \hat{I}_{int}(k, m\delta z_D).$$
 (4)

Eq. (4) reveals that the GD-fusion can also be performed in the spectral domain by convoluting some appropriate sliding spectral Gabor windows, i.e. $\Im^{-1}\{g(z_D-m\delta z_D)\}$, with each spectral interference signal acquired at different focus positions of the objective lens. In practice, the convolution term in Eq. (4) is equivalent to performing a band-pass filter on a spectral interference signal [17]. The filtered spectral interference signals are then summed to form a final fused spectral interference signal that contains only in-focus signal from each acquired raw spectrum. Finally, by Fourier transform of the final fused spectra, a cross sectional image that contains in-focus detail across the

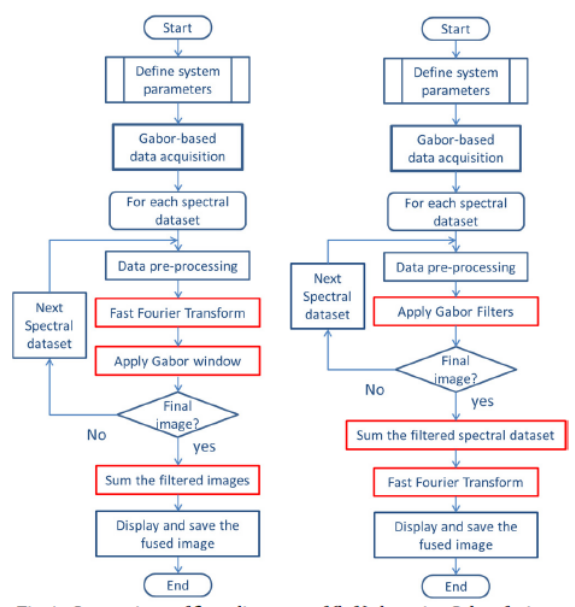


Fig. 1. Comparison of flow diagrams of (left) the prior Gabor fusion and (right) the spectral Gabor fusion methods.

desired imaging depth similar to that achieved in [11] can be obtained. We refer to this fusing method as "spectral-domain GD-fusion". The new fusing method is expected to improve the processing speed of the GD-OCM since only one Fourier transformation per one depth scan is required as oppose to multiple Fourier transformation per one depth scan in the original GD-OCM. Fig. 1 shows comparison of the flow diagram of the spectral fusion method as compared with the original approach in [11].

To experimentally verify the speed improvement, the new spectral fusing method and the prior spatial fusing method were implemented in LabVIEW programming environment (National Instrument, USA) by following the flow charts shown in Fig. 1. The processing host was a desktop computer with Intel Core i5, 3.1 GHz CPU, 16 GB memory, and under 64 bits operating system running Window 7 Professional. From Fig. 1, since there is no difference in data acquisition for both methods, only processing times were compared and presented. Therefore, a set of GD-OCM data that was pre-acquired and stored in the computer's hard drive was used for the study. The number of GD-samples was 5 images that were acquired at every 100 microns focal shift interval along depth. Each GD sample consisted of 1000 spectra per frame. Each spectrum was acquired at a sampling resolution of 3600 points per spectrum. To compare the performance of both methods for different sizes of spectra, the acquired spectra were then down sampled to the sizes of 500, 1000, 1500, 2000, 2500, 3000, and 3500 points per spectrum as shown in Table 1. All processes were kept the same between the two methods except those in the red box shown in Fig. 1, which are the fusion process and the fast Fourier transform (FFT). In each table, the FFT size was kept the same for both methods for a given

The implementation of the spatial-domain GD-fusion followed the same procedure as presented in [11]. While we previously showed that the spatial-domain GD-fusion is capable of adaptive filtering for different types of samples, here we will assume the same type of samples in comparing the two approaches, and as such in both cases pre-optimized filters will be considered. Therefore, the fusing process of the spatial-domain GD-fusion involves multiplication of each acquired image with

a corresponding pre-optimized Gabor window and summation of all filtered images to obtain the final fused image. On the other hand, the spectral-domain GD-fusion involves application of each acquired spectrum with a pre-optimized band-pass filter and summation of all filtered spectra to obtain the final fused spectrum. The final fused image was obtained by Fourier transformation of the fused spectra.

Fig. 2 illustrates the process of the spectral-domain GD-fusion. Fig. 2(a-e) are examples of the raw spectra acquired at different focus position inside the sample. In this demonstration, a Chebyshev digital band-pass filter was implemented for the spectral filtering [17]. Fig. 2(f-j) shows example of the filtered spectra. As for verification of the filtering process, Fig. 2(k-o) demonstrates their corresponded cross-sectional images obtained by FFT of each frame of the filtered spectra. Fig. 2(p) is an example of a combined (or spectrally fused) spectrum. Fig. 2(q) shows the final fused image obtained from the FFT of a frame of fused spectra. It should also be pointed out that the spectral fusing method also provides DC removal in the process, which is a necessary preprocessing step for the spatial-domain fusion.

Processing times of both methods, i.e. only those processes marked by the red box in Fig. 1, were measured and compared for the case of 2048 and 4096 FFT sizes as shown in Table 1 and Table 2 respectively, to keep the FFT sizes in powers of 2 assuming the spectra sizes vary in a range of 500 to 3500 points, which is a common practice for obtaining sufficient sampling points of the depth profile in FD-OCT regardless of the acquired spectrum size. Moreover, Table 3 compares the processing times when the FFT size matches the size of the spectra. Each processing time in all tables is presented as mean \pm standard deviation as computed from 10 measurements (N =10) for each case.

Table 1 Comparison of the processing times of a spatial-domain GD-fusion method versus the spectral-domain GD-fusion when

the FFT size was fixed to 2046 points			
Spectrum	FFT size	Total processing time (ms)	
size	(points)	Spatial-domain	Spectral-domain
(pixels)		GD-fusion	GD-fusion
500	2048	202.0 ± 0.7	86.9 ± 1.3
1000	2048	214.3 ± 1.1	131.6 ± 1.3
1500	2048	227.4 ± 1.0	177.0 ± 1.2
2000	2048	239.0 ± 0.9	219.3 ± 0.8
2500	2048	242.1 ± 0.9	264.6 ± 1.9
3000	2048	255.5 ± 1.2	308.6 ± 2.1
3500	2048	272.8 ± 1.4	358.5 ± 2.1

Table 2 Comparison of the processing times of the spatial-domain GD-fusion versus the spectral-domain GD-fusion when the FFT

size was fixed to 4096 points			
Total processing time (ms)			
nain			
n			
.3			
.2			
.1			
.3			
.5			
.7			
.8			

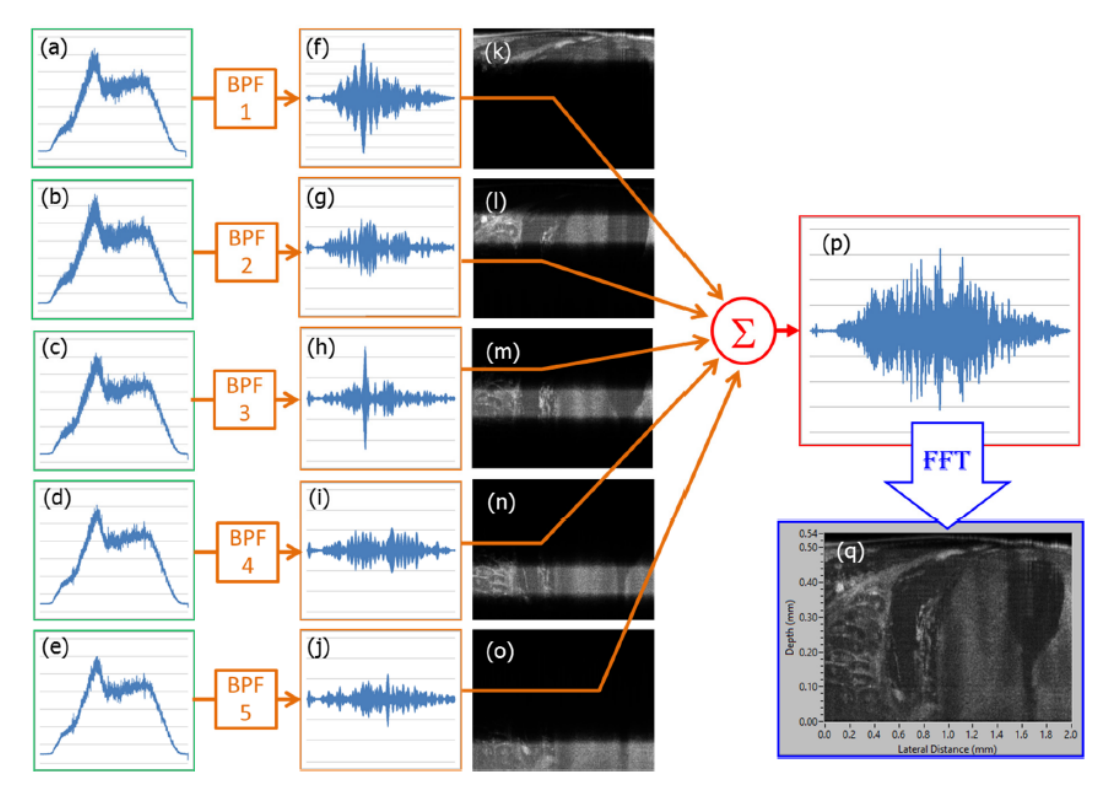


Fig. 2. Examples of (a-e) acquired raw spectra at different focus position along the depth, (f-j) filtered spectra, (k-o) filtered images correspond with each filtered spectra, (p) a fused spectrum as a result of summation of all filtered spectra, and (q) the final fused image obtained by performing the fast Fourier transform of the fused spectrum in (p). (BPF = band-pass filter)

Table 3 Comparison of the processing times of the spatial-domain GD-fusion versus the spectral-domain GD-fusion when the FFT size was kept the same with the spectrum size.

size was kept the same with the spectrum size.			
Spectrum	FFT	Total processing time (ms)	
size	size	Spatial-domain	Spectral-domain
(pixels)	(points)	GD-fusion	GD-fusion
500	500	68.3 ± 0.7	63.3 ± 1.2
1000	1000	121.2 ± 0.8	115.1 ± 0.9
1500	1500	181.4 ± 1.0	171.8 ± 1.2
2000	2000	232.2 ± 0.8	221.1 ± 1.0
2500	2500	301.7 ± 2.2	276.7 ± 1.3
3000	3000	348.6 ± 2.2	329.9 ± 2.1
3500	3500	430.7 ± 2.5	387.5 ± 2.0

Results show that, in the cases of fixed 4096 points FFT (Table 2), the spectral-domain GD-fusion outperforms the spatial-domain GD-fusion. Specifically, when the spectrum size is less than 1500 points, the processing time of the spectral-domain GD-fusion is more than twice as fast as that of the spatial-domain GD-fusion. This scenario occurs when high axial resolution is demanded, requiring FFT sizes that correspond to at least double sampling of the axial point spread function (PSF)) for a given depth. For example, imaging 500 μm deep in skin with a 1 μm axial PSF requires about 4000 points FFT if the PSF is sampled with four points. The processing only takes more time when the spectrum is down sampled through the FFT sizing process, which is not typical. In the cases when the FFT size is the same with the spectrum, the processing speed of both spatial fusing and spectral fusing methods are almost the same while the spectral fusing method is slightly faster as shown in Table 3. Also this case is perhaps more typical but not desirable in many instances where for example high definition boundaries are required and high sampling of the PSF is preferred.

In conclusion, we presented a spectral fusing technique for GD-OCM that is based on Gabor filtering and fusion in the spectral domain. The proposed technique shows improved speed for high definition sampling in the spatial domain compared to the spatial-fusion technique. To date, a commonly used spectrum size in our GD-OCM imaging system is about 1000 points per spectrum, processed with a 4096 points FFT, which is largely sufficient for imaging across the depth of 1 mm at equivalent 0.5 µm sampling of a 2 µm axial PSF, and equivalently 1 µm sampling for a 2048 points FFT. In both cases, the spectral-domain fusion is about twice as fast as the spatial-domain fusion. Furthermore, it is worth noting that a hardware implementation of the processing algorithm is possible by utilizing hardware-based signal processing, such as an FPGA enabled frame grabber [18] or other similar acquisition devices. The hardware-based filtering is expected to greatly improve the processing speed of the presented spectral fusing method, which will be further investigated in the future.

Funding. Thailand Research Funds (TRF) (TRG5680091)

References

- D. Huang, E. A. Swanson, C. P. Lin, J. S. Schuman, W. G. Stinson, W. Chang, M. R. Hee, T. Flotte, K. Gregory, C. A. Puliafito, and J. G. Fujimoto, Science 254, 1178 (1991).
- J. A. Izatt, M. R. Hee, G. M. Owen, E. A. Swanson, and J. G. Fujimoto, Opt. Lett. 19, 590 (1994).
- 3. W. Drexler, U. Morgner, F. X. Kartner, C. Pitris, S. A. Boppart, X. D. Li, E. P. Ippen, and J. G. Fujimoto, Opt. Lett. 24, 1221 (1999).
- A. D. Aguirre, P. Hsiung, T. H. Ko, I. Hartl, and J. G. Fujimoto, Opt. Lett. 28, 2064 (2003).
- 5. J. M. Schmitt, S. L. Lee, and K. M. Yung, Opt. Comm. 142, 203 (1997).
- M. Avanaki, A. Hojjatoleslami, M. Sira, J. B. Schofield, C. Jones, and A. G. Podoleanu, Appl. Opt. 52, 2116 (2013).

- J.P. Rolland, P. Meemon, S. Murali, A. Jain, N. Papp, K. P. Thompson, et al., Proc. SPIE 7139, 71390F (2008).
- A. F. Fercher, C. K. Hitzenberger, G. Kamp, and S. Y. El-Zaiat, Opt. Comm. 117, 43 (1995).
- 9. S. Murali, K. S. Lee, and J. P. Rolland, Opt. Express 15, 15854 (2007).
- 10. S. Murali, K. Thompson, and J. Rolland, Opt. Lett. 34, 145 (2009).
- J.P. Rolland, P. Meemon, S. Murali, K. P. Thompson, and K. S. Lee, Opt. Express 18, 3632 (2010).
- 12. P. Bouchal, A. Bradu, and A.G. Podoleanu, Opt. Express 20, 5368 (2012)
- K. S. Lee, K. P. Thompson, P. Meemon, and J. P. Rolland, Opt. Lett. 36, 2221 (2011).
- K.-S. Lee, H. Zhao, S. F. Ibrahim, N. Meemon, L. Khoudeir, and J. P. Rolland, J. Biomed. Opt. 17, 126006 (2012).
- P. Tankam, Z. He, Y.-J. Chu, J. Won, C. Canavesi, T. Lepine, H. B. Hindman, D. J. Topham, P. Gain, and G. Thuret, Opt. Lett. 40, 1113 (2015).
- P. Tankam, A. P. Santhanam, K.-S. Lee, J. Won, C. Canavesi, and J. P. Rolland, J. Biomed. Opt. 19, 071410 (2014).
- J. V. D. Vegte, Fundamentals of Digital Signal Processing (Prentice Hall PTR, 2001).
- T. E. Ustun, N. V. Iftimia, R. D. Ferguson, and D. X. Hammer, Rev. Sci. Instr. 79, 114301 (2008).